Modeling Junctions in Sharp Edge Conducting Structures With Higher Order Method of Moments

Modeling Junctions in Sharp Edge Conducting Structures with Higher Order Method of Moments

Guido Lombardi, *Senior Member, IEEE*, Roberto D. Graglia, *Fellow, IEEE*

***Abstract*—Scattering targets are often made by complex structures constituted by thin metallic plates as wings, fins, winglets. When thin plates are connected together, they define surface junctions with the possible presence of sharp edges.**

In this paper we describe a complete procedure to handle junctions in presence of sharp edges in surface integral equation methods by defining the required basis functions and unknowns. This approach is based on the use of divergence-conforming higher order interpolatory vector basis functions, singular vector basis functions and on Kirchhoff's Current Law. The paper presents several numerical test cases that show the instability of solutions using classical methods and the full convergence of the proposed numerical scheme.

***Index Terms*—Integral equations, method of moments (MoM), electromagnetic diffraction, edges, junctions, singular vector functions, higher order modeling, Kirchhoff's Current Law.**

I. Introduction

SIMPLE sharp edge structures have been studied in the past by using the method of moments (MoM) with additive high-order interpolatory [1] and singular [2] divergence-conforming triangular basis functions [2]-[7]. However, high-order bases have not yet been used to model *junction* problems where plates are attached to piecewise-planar or curved surfaces. Until now, junctions were typically modeled by using classical low-order MoM schemes [8]-[13] with *ad hoc* modifications of the so called Rao-Wilton-Glisson (RWG) basis functions [14]. Unfortunately, low-order schemes are unable to model the singular behavior of the charge and current densities on sharp-edges [15], [16], with field singularities that might be present in the neighborhood of the edges of two or more wedges attached together. To improve on these models, in this paper we approach the junction problem by using the high-order singular divergence-conforming vector bases of *additive* kind developed for triangular cells in [5], because these bases are able to model the electromagnetic singularities in the neighborhood of sharp edges. Our aim is to model the junction and avoid unphysical oscillations in the numerical solution.

The high-order singular bases are formed by the union of two sub-sets: a vector sub-set of *interpolatory* basis functions that is complete to an arbitrarily high order p plus a *Meixner* sub-set formed by singular vector basis functions. In turn, the Meixner subset is obtained by multiplying the lowest order singular basis functions of [5, Table I] times an s-th order complete interpolatory polynomial set [5]. Recall that the additive scheme in [5] augments the number of the degrees of freedom of each triangular element attached to a sharp edge; these are either edge- or vertex-singular elements (see [5, Fig. 1]) on which, for example, the triangular lowest-order singular basis functions of [5, Table I] are defined.

G. Lombardi and R.D. Graglia are with the Dipartimento di Elettronica e Telecomunicazioni, Politecnico di Torino, 10129 Torino, Italy e-mails: guido.lombardi@polito.it, roberto.graglia@polito.it.

Manuscript received May -, 2014.

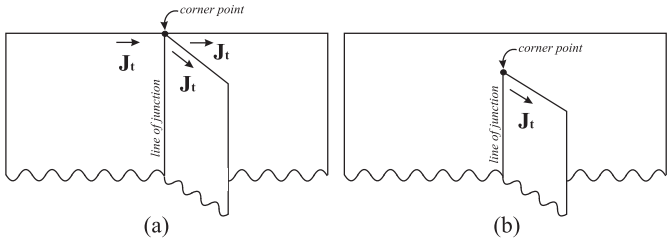

Fig. 1. (a) Plate-to-plate junction; (b) plate-to-surface junction.

As discussed below, the use of interpolatory basis functions simplifies the junction model because only one basis function per triangle does not vanish on a given interpolation point lying on an edge in common to several triangular cells.

For the sake of brevity, in the following we limit our investigation to knife-edge singularities where one is faced with the two different problems:

a) plate-to-plate junctions;
b) plate-to-surface junctions;

that are illustrated in Fig. 1. We do this without loss of generality because, in spite of their strikingly simple geometries, both the junctions of Fig. 1 contain a corner-point. In fact, more precisely, one of the major numerical difficulties is in modeling the current density at the corner-point where one cannot resort to any analytical method to predict the current density behavior. On the (infinitely thin) plates shown in Fig. 1, the component $\boldsymbol{J}_t$ of the current density tangent to the edge-profiles could be unbounded (infinite) at the edges, and be unbounded also at the *corner-point* indicated in the figure. It is clear that to guarantee the current continuity in the neighborhood of the corner-point in case of plate-to-plate junctions (Fig. 1a) one needs a different approach from the one used to deal with plate-to-surface junctions, where the infinite current density running along the edge has to flow out on a locally flat surface at the corner-point.

The procedure to numerically impose the current continuity at a junction when using high-order singular triangular elements is described in Section II, and then validated by the results obtained for the plate-to-plate and the plate-to-surface junction reported in Section III and IV, respectively. These two Sections consider canonical T-shape surface junctions (Fig. 1a, b) and provide a physical interpretation of the numerical

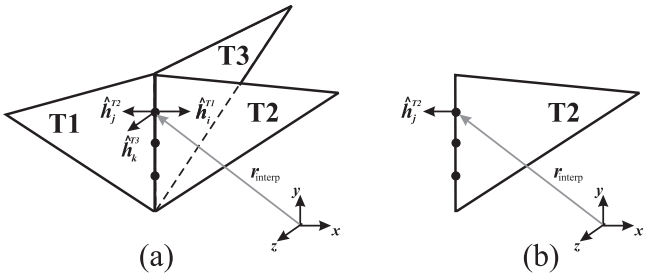

Fig. 2. Three triangular cells (T1, T2, and T3) with a common edge along the line of junction. (a) The common edge has global edge number e and local edge number indicated by the dummy index i, j and k for the triangle T1, T2 and T3, respectively. (b) $\hat{\boldsymbol{h}}_j^{\mathrm{T2}}$ is the outward unit normal to the j-th edge of T2 evaluated at the interpolation point $\boldsymbol{r}_{\mathrm{interp}}$ in common to the three triangles.

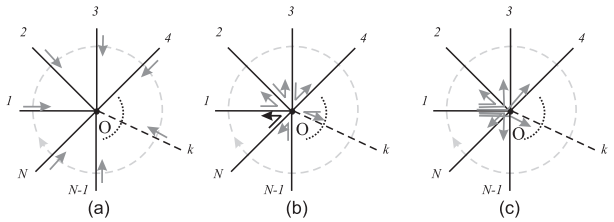

Fig. 3. Junction cross-sectional view. The *interpolatory* point (O) is in common to N triangular patches that share a common edge along a line (locally) normal to the plane of the sheet (that is, the line of junction). (a) The arrows show, for each patch and at the interpolation point, the component of the current density $\boldsymbol{J_k}$ normal to the line of junction. (b, c) Two different ways to select independent DOFs at the interpolation point (see also [8]-[12]).

results obtained for the current density by using high-precision numerical tools [17], [18]. Conclusions are reported in Section V. Readers may find it helpful to review [1], [2], [5] and references therein for background information.

II. Current Continuity at a Junction

The procedure to impose the continuity of the current density at a junction when using high-order vector basis functions is better discussed by considering the simple example shown in Fig. 2, where three triangular cells (T1, T2, and T3) share a common edge along the "line of junction" departing from the *corner-point* of Fig. 1. The cell edges are *globally* numbered from 1 to n_e (n_e=7 in Fig. 2) and *locally* numbered from 1 to 3 on each given cell. The common edge of Fig. 2 has global edge number e and local edge number indicated by the dummy index i, j and k for the triangle T1, T2 and T3, respectively. Recall also that on each point of a triangular cell we define three (local) height unit vectors ($\hat{\boldsymbol{h}}_1$, $\hat{\boldsymbol{h}}_2$, $\hat{\boldsymbol{h}}_3$), each one associated with a different edge bounding the cell (that is, edge 1, 2 or 3, respectively) [1]. The height vectors are tangent to the cell surface and, on the ℓ–th edge, $\hat{\boldsymbol{h}}_\ell$ is the outward unit normal to the element [1]. For example, with reference to Fig 2, $\hat{\boldsymbol{h}}_j^{\mathrm{T2}}$ is the outward unit normal to the j-th edge of T2 (the e–th global edge) evaluated at the interpolation point $\boldsymbol{r}_{\mathrm{interp}}$ in common to the three triangles of Fig. 2. Similarly, at the same interpolation point of the e–th global edge, $\hat{\boldsymbol{h}}_i^{\mathrm{T1}}$ is the outward unit normal to the i-th edge of T1 and $\hat{\boldsymbol{h}}_k^{\mathrm{T3}}$ is the outward unit normal to the k-th edge of T3.

Charge accumulation along the edge in common to T1, T2 and T3 is simply avoided by imposing the Kirchhoff Current Law (KCL) in terms of the current density $\boldsymbol{J}$ and of the MoM degrees of freedom (DoF) [14]. This is conveniently done by separating the current density

$$\boldsymbol{J} = \boldsymbol{J}_{\mathrm{poly}} + \boldsymbol{J}_{\mathrm{meix}} \tag{1}$$

into its polynomial ($\boldsymbol{J}_{\mathrm{poly}}$) and singular Meixner part ($\boldsymbol{J}_{\mathrm{meix}}$), and by recalling that along the common edge there are $(p+1)$ interpolation points associated with the vector polynomial subset of order p, and $(s+1)$ interpolatory points associated with the singular Meixner subset of order s. On each interpolation point along the common edge, the edge-normal current component is always finite because all the edge-interpolation

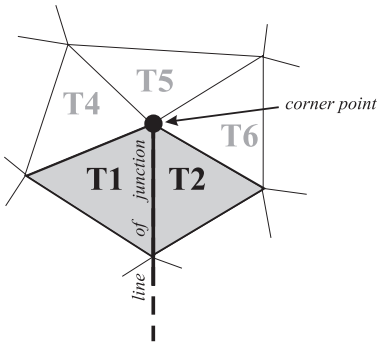

Fig. 4. Plate-to-surface junction. The triangle T3 lies on a plane different from the one containing T1 and T2.

points are located in the edge interior [1], [5]. In this manner, KCL yields the following $(p+s+2)$ conditions

$$\boldsymbol{J}_{\mathrm{poly}}^{\mathrm{T1}} \cdot \hat{\boldsymbol{h}}_i^{\mathrm{T1}} + \boldsymbol{J}_{\mathrm{poly}}^{\mathrm{T2}} \cdot \hat{\boldsymbol{h}}_j^{\mathrm{T2}} + \boldsymbol{J}_{\mathrm{poly}}^{\mathrm{T3}} \cdot \hat{\boldsymbol{h}}_k^{\mathrm{T3}} = 0 \tag{2}$$

$$\boldsymbol{J}_{\mathrm{meix}}^{\mathrm{T1}} \cdot \hat{\boldsymbol{h}}_i^{\mathrm{T1}} + \boldsymbol{J}_{\mathrm{meix}}^{\mathrm{T2}} \cdot \hat{\boldsymbol{h}}_j^{\mathrm{T2}} + \boldsymbol{J}_{\mathrm{meix}}^{\mathrm{T3}} \cdot \hat{\boldsymbol{h}}_k^{\mathrm{T3}} = 0 \tag{3}$$

with (2) holding on $(p+1)$ interpolation points of the vector polynomial subset and (3) on $(s+1)$ interpolation points associated with the singular Meixner subset. Conditions (2) and (3) reduce the number of degrees of freedom of the problem. As explained in [1], the high-order interpolatory vector basis functions $\boldsymbol{\Lambda}^\ell$ used to expand on each triangle T the polynomial part of the current $\boldsymbol{J}_{\mathrm{poly}}^{\mathrm{T}}$ are normalized to ensure that the component of $\boldsymbol{\Lambda}^\ell$ along $\hat{\boldsymbol{h}}_\ell$ at the interpolation point is unity. Because of the used normalization, it is clear that, at each interpolation point on the line of junction of Fig. 2, (2) simply relates three unknown expansion coefficients to each other. The same holds for (3), although the Meixner vector basis functions are normalized in a different manner and the interpolation points of the Meixner part could be different from those of the regular (polynomial) part. The results of the previous example are readily extended to more complex situations, since the number of terms adding up on the left-hand side of (2, 3) is equal to the number of cells that share the same common edge. As schematically depicted in Fig. 3, several different ways based on (2) can be used to impose the current continuity at junctions when using low-order RWG basis functions, see also [8]-[12].

To the best of our knowledge, a closed-form solution for the current density at the corner point of junctions of the kind

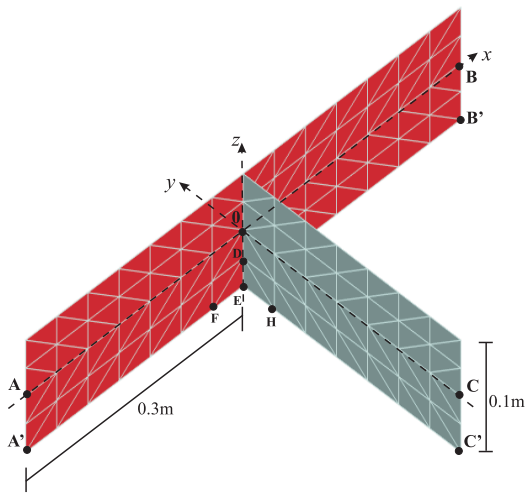

Fig. 5. T-shape surface formed by joining three zero-thickness rectangular plates of size $0.1\text{m} \times 0.3\text{m}$. The structured mesh **S** shown in the figure consists of 168 right-angled triangles of equal size. 0 is the origin of the Cartesian reference frame; $A = (-0.3, 0, 0)$, $B = (0.3, 0, 0)$, $C = (0, -0.3, 0)$ [m].

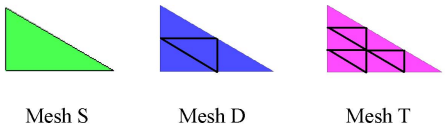

Fig. 6. Each cell of the original **S**-mesh is subdivided into 4 and 9 triangular cells to define the denser **D**- and **T**-mesh.

shown in Fig. 1a,b is not available in the literature; thus we focus our attention on how to model the current density on the line of junction constituted by knife-edges. The geometry of the plate-to-plate junction of Fig. 1a is however similar to that of Fig. 2; in this case, the triangular elements attached to the corner point of Fig. 1a can be defined as in Fig. 2.

Conversely, for plate-to-surface junctions (Fig. 1b), different heuristic approaches based on the additive nature of our basis functions can be used. Once again, these are better illustrated using a simple example, shown in Fig. 4. In this case the "corner point" is the common node of several triangular cells of the (locally flat) surface that drains the infinite current density coming from the sharp edge. The edge in common to the triangle T1 and T2 is along the "line of junction" and there is a third triangle T3 (not shown in the figure) that lies on a plane different from the one containing T1 and T2 and that shares the same common edge. The sharp edge is attached to the corner point and lies on the plane of T3; T3 is a singular element.

In Fig. 4 the cells T1, T2, T4, T5, and T6 have a vertex in common at the corner point and, on the surface defined by these cells, the current density can be singular at the corner point. On the locally flat surface, the current density can be modeled

- by partially reducing the singular Meixner basis function subsets [5] used on the singular cell T3 to model the junction only with regular bases (in this case, all the elements from T1 to T6 are regular elements while T3 is a *lacunary* edge-singular element);

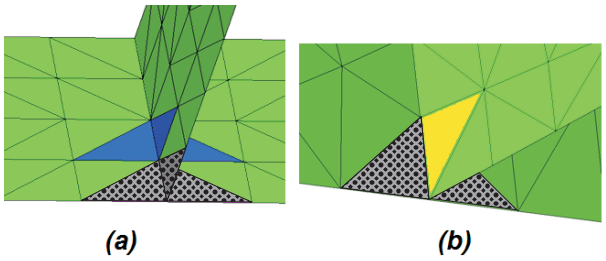

Fig. 7. (a) Three edge singular elements connected to the line of junction (dotted-gray), three regular elements connected to the line of junction (blue), (b) three singular elements connected to the line of junction (edge singular elements in dotted-gray, vertex singular element in yellow).

- or by partially increasing with vertex singular Meixner basis functions the polynomial sub-sets used in the T1 and T2 cells attached to the line of junction, (in this case, T4, T5, and T6 are regular elements, and T3 is an edge-singular element).

The latter approach is the one proposed in this paper for plate-to-surface junctions and the elements (T1 and T2) obtained in this manner are defined *lacunary* vertex singular elements. This choice is justified by the fact that our aim is to model how a knife-edge merges into a regular surface. This approach is validated in Section IV by several numerical results relative to a test-case problem already considered in [9]; the convergence of our numerical procedure is assessed by physical interpretation of the results.

III. Plate-to-plate Junction Structures

To illustrate the effectiveness of the modeling scheme of Section II we first consider the test-case shown in Fig. 5 that in [9] has been studied by using (low-order) RWG basis functions. Extension to more general cases is straightforward. The T-shape surface of Fig. 5 is the union, along the line of junction $\{x = 0, y = 0, -0.05 < z < 0.05)\}$, of three zero-thickness rectangular plates $0.1\text{m} \times 0.3\text{m}$ in size. The T-shape surface is discretized in Fig. 5 with 168 right-angled triangular cells of the same size (mesh **S**). By subdividing each cell of the **S**-mesh into 4 and 9 triangular cells, as shown in Fig. 6, we easily define a denser **D**- and **T**-mesh, consisting of 672 and 1512 cells, respectively.

Notice that along the line of junction one encounters several combinations of regular/singular elements. Fig. 7 shows triplets of elements with a common edge along the line of junction. In particular, Fig. 7a highlights three edge singular elements (dotted-gray) and three regular elements (in blue) attached to the line of junction, while Fig. 7b shows two edge-singular elements (dotted-gray) and one vertex-singular element (yellow) attached to the line of junction.

In the rest of this Section we present several numerical results obtained by solving in frequency domain the electric field integral equation (EFIE) with the method of moments and the Galerkin approach. With reference to [9], the T-shape structure is excited in free space by a linearly polarized plane wave

$$\boldsymbol{E}^{inc} = \boldsymbol{E}_0 \exp\left(jk_o \hat{\boldsymbol{k}}^i \cdot \boldsymbol{r}\right) \exp\left(-j\omega t\right) \qquad (4)$$

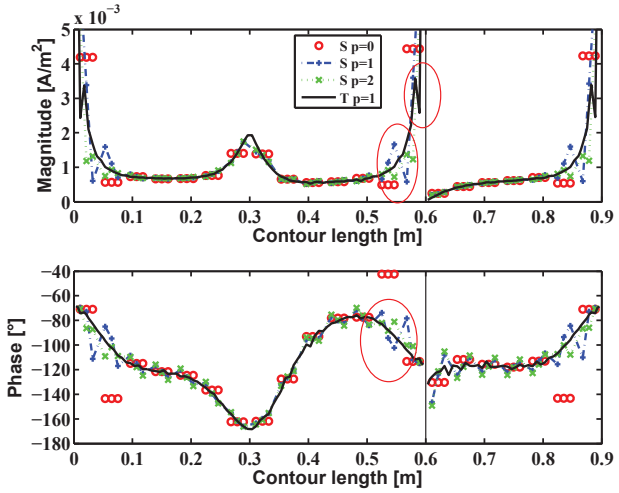

Fig. 8. Purely polynomial bases results. Magnitude and phase of the current density J_z along the line $A \to B$ and $0 \to C$ shown in Fig. 5. The contour points at 0m, 0.3m, 0.6m and 0.9m correspond to point A, 0, B and C of Fig. 5 respectively. The ellipses highlight the spurious oscillations near point B. Similar oscillations occur near A and C. The current is induced by a 300MHz plane wave with $\theta^i = 45°$, $\varphi^i = 45°$, and $\boldsymbol{E}_0 = 1\hat{\boldsymbol{\theta}}$ [V/m]. The figure compares four results obtained by using different meshes and element order: mesh **S** with regular elements of order $p = 0$, $p = 1$, $p = 2$ and mesh **T** with regular elements of order $p = 1$.

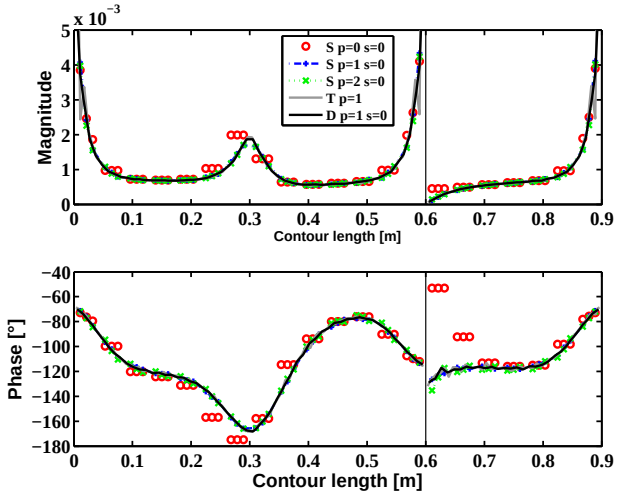

Fig. 9. Singular element results for the test case considered in Fig. 8 obtained by using different meshes and element orders: Mesh **S** with singular elements of order $p = 0, s = 0$, $p = 1, s = 0$, $p = 2, s = 0$, Mesh **D** with singular elements of order $p = 1, s = 0$ and Mesh **T** with regular elements of order $p = 1$.

with

$$\hat{\boldsymbol{k}}^i = -\left(\hat{\boldsymbol{x}}\cos\varphi^i \sin\theta^i + \hat{\boldsymbol{y}}\sin\varphi^i \sin\theta^i + \hat{\boldsymbol{z}}\cos\theta^i\right) \qquad (5)$$

and $\boldsymbol{r} = [x, y, z] = r[\sin(\vartheta)\cos(\varphi), \sin(\vartheta)\sin(\varphi), \cos(\vartheta)]$.

To highlight the singular behavior of the electromagnetic field and current, we first analyze the structure at a low frequency $f = 300$MHz, where each plate of the T-structure is $0.3\lambda \times 0.1\lambda$ in size.

The structure is illuminated by the same plane wave considered in [9], with parameters $\theta^i = 45°$, $\varphi^i = 45°$, and

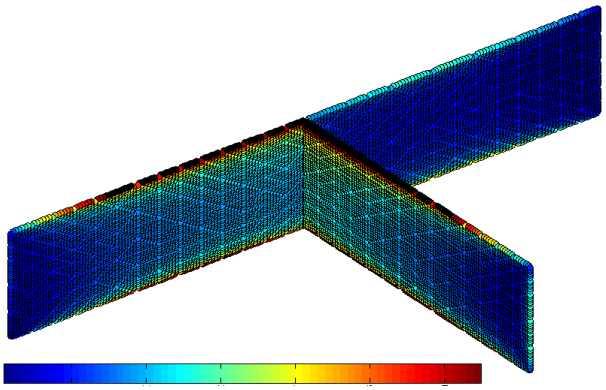

Fig. 10. L2-norm of the current density $\boldsymbol{J}$ induced on the T-shape structure by a plane wave with $\theta^i = 45°$, $\varphi^i = -75°$ and $\boldsymbol{E}_0 = 1\hat{\boldsymbol{\theta}}$ [V/m] @300MHz when singular basis functions of order $p = 2, s = 0$, junction modeling and mesh **D** are used. Color version of this figure is available online at http://ieeexplore.ieee.org.

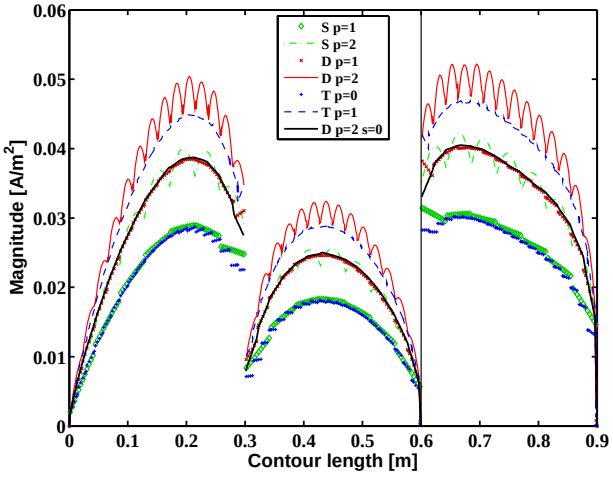

Fig. 11. T-shape structure at 300MHz. Magnitude of current density component tangent to the contour lines $A' \to B'$ and $E \to C'$ and sampled at a distance of $\lambda/1000$ in z direction from the border of the structure, see also Fig. 5. Simulations obtained with regular elements and different meshes are compared with the reference simulation obtained with mesh **D** and singular basis functions of order $p = 2, s = 0$.

$\boldsymbol{E}_0 = 1\hat{\boldsymbol{\theta}}$ [V/m]. Fig. 8 and 9 show the magnitude and phase of the current component J_z along the contour line $A \to B$ and $0 \to C$ shown in Fig. 5. The contour points at 0m, 0.3m, 0.6m and 0.9m correspond respectively to point A, 0, B and C of Fig. 5. Various results obtained by using only regular (polynomial) elements are compared in Fig. 8 while Fig. 9 shows the solutions obtained by using singular elements. As expected, the results of Fig. 8 obtained with regular bases show spurious oscillations of magnitude and phase in the region near the sharp edge profile [5]. The reference (best) solution is the one shown in Fig. 9, obtained with mesh **D** and singular basis functions of order $(p = 1, s = 0)$. Notice that on the $y = 0$ plane, the current density J_z is continuous from the first to the second plate and equal to zero on the 3rd plate at $x = 0$.

The results that follow are relative to the same structure of Fig. 5 illuminated by a 300MHz plane wave with a different

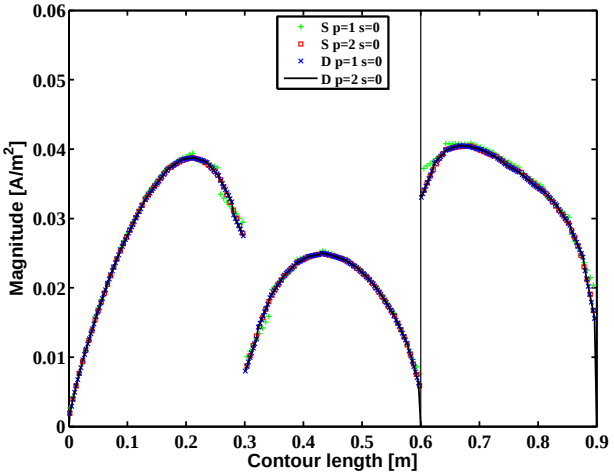

Fig. 12. Study of convergence of the magnitude of current density component defined in Fig. 11 using singular basis functions and different meshes.

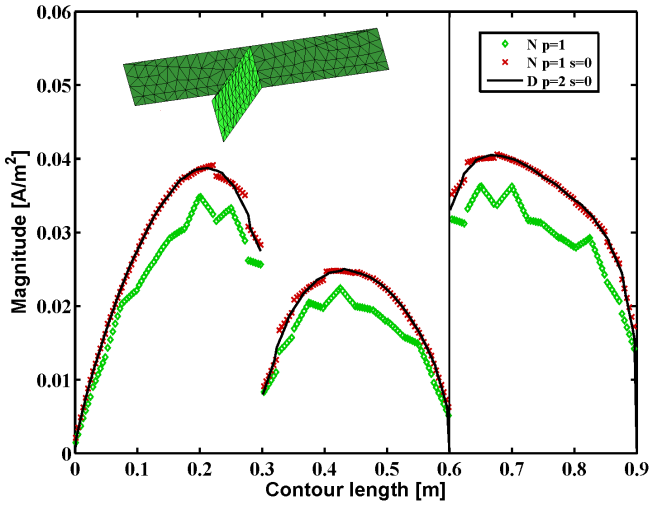

Fig. 13. Study of convergence of the magnitude of the current density component defined in Fig. 11 using regular and singular basis functions together with the structured mesh **D** and the unstructured mesh **N** (shown in the inset) consisting of 329 elements.

incident direction ($\theta^i = 45°$, $\varphi^i = -75°$, $\boldsymbol{E}_0 = 1\hat{\boldsymbol{\theta}}$). For this incidence, the current density at the junction is different from zero on all the three plates. Fig. 10 shows the L2-norm of the current density $\boldsymbol{J}$ computed with mesh **D** and singular basis functions of order $(p = 2, s = 0)$. The solution is shown by using small colored circles and by sampling the results on a grid of points, without using any post-processing visualization artifact that could artificially improve the data rendering. A 64 color-scale (dark blue=1st level, dark red=last level) is adopted with saturation level set to 0.035A/m^2. The maximum value of the sampled data is 0.0695A/m^2 which is over the saturation value. The values above saturation are reported in black. The number of sampling points per cell is 21 and they are chosen never to lie on edges or vertexes of the triangular cells, where the numerical solution could be discontinuous (across elements boundaries) or unbounded, as it happens on the plate edges

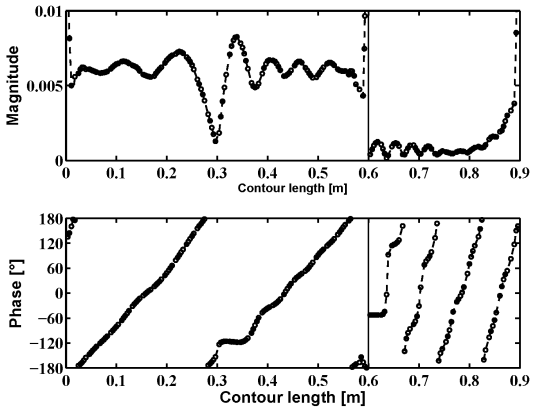

Fig. 14. T-shape structure at 6GHz. Magnitude and phase of the current density J_z along the contour line $A \to B$ and $0 \to C$ shown in Fig. 5. Simulation is performed using singular elements of order $p = 2, s = 0$ and mesh **D**.

when using singular elements.

Figs. 11 and 12 show the current density component tangent to the contour lines $A' \to B'$ and $E \to C'$ (Fig. 5) and sampled at a distance of $\lambda/1000$ in the z direction from the border of the structure. This component is strongly affected by the bifurcation of the structure, being normal to the line of junction. Fig. 11 shows that the use of regular basis functions with junction condition enforcement is unable to model the physics of the problem, since it provides unstable solutions with a lot of unphysical oscillations and with a wrong scale of magnitude. Conversely, Fig. 12 shows that by using singular bases together with junction modeling one gets stable convergent solutions.

Fig. 13 shows that convergence is preserved also by using unstructured meshes (this figure shows in the inset the used mesh **N**, with 329 elements).

Moreover, good physical solutions are obtained also for larger structures (in terms of wavelength). For example, the results of Fig. 14 are relative to the T-shape structure shown in Fig. 5 illuminated by a 6GHz incident plane wave with $\theta^i = 45°$, $\varphi^i = -75°$ and $\boldsymbol{E}_0 = 1\hat{\boldsymbol{\theta}}$ [V/m]. In this case each rectangular plate is $2\lambda \times 6\lambda$. The problem is numerically studied with mesh **D** and singular basis functions of order $(p = 2, s = 0)$. Fig. 14 reports the J_z magnitude along the contour line $A \to B$ and $0 \to C$ (see Fig. 5).

Table I reports details on the number of DOFs for all the simulations reported in this Section (in agreement with the discussion reported in Section II).

IV. Plate-to-surface Junction Structures

To illustrate the modeling procedure for plate-to-surface junctions we consider a convenient test-case, as already done in the previous section. The structure shown in Fig. 15 is a modified version of the T-shape junction described in Section III: only the width of one of the rectangular plates is modified from 0.1m to 0.05m. Fig. 15 shows mesh **S** constituted by

TABLE I
NUMBER OF DOFS IN SIMULATIONS OF SECTION III

Bases and Mesh	DOFs	Figure
p=0, mesh **S**	227	Fig. 8
p=1, mesh **S**	790	Figs. 8,11
p=2, mesh **S**	1689	Figs. 8,11
p=1, mesh **D**	3260	Fig. 11
p=2, mesh **D**	6906	Fig. 11
p=0, mesh **T**	2193	Fig. 11
p=1, mesh **T**	7410	Figs. 8,9,11
p=0,s=0, mesh **S**	365	Fig. 9
p=1,s=0, mesh **S**	929	Figs. 9,12
p=2,s=0, mesh **S**	1828	Figs. 9,12
p=1,s=0, mesh **D**	3561	Figs. 9,12
p=2,s=0, mesh **D**	7207	Figs. 10-14
p=1, mesh **N**	1566	Fig. 13
p=1,s=0, mesh **N**	1805	Fig. 13

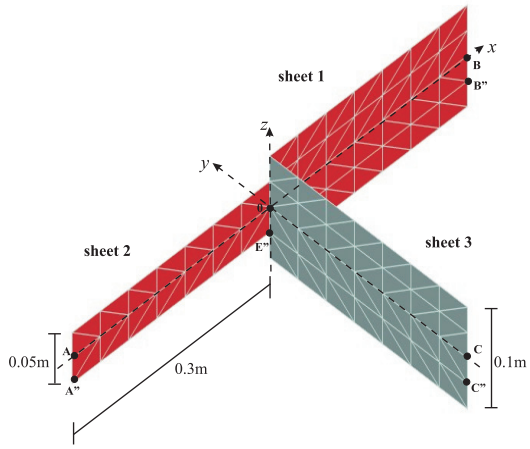

Fig. 15. Modified T-shape surface discretized with the structured mesh **S** consisting of 140 right-angled triangular cells of equal size. 0 is the origin of the Cartesian reference frame; $A = (-0.3, 0, 0)$, $B = (0.3, 0, 0)$, $C = (0, -0.3, 0)$, $A" = (-0.3, 0, -0.025)$, $B" = (0.3, 0, -0.025)$, $C" = (0, -0.3, -0.025)$ [m].

140 right-angled triangular cells of the same size. We also define denser **D**- and **T**-mesh, where each triangle of **S**-mesh is subdivided respectively into 4 and 9 cells (see Fig. 6), thereby obtaining a mesh with 560 and 1260 elements.

As stated at the end of Section II, in order to correctly model the behavior of the current density in the region near the corner point of a plate-to-surface junction, we can either partially add singular bases to regular elements or partially remove singular bases from singular elements in cells connected to the corner point (see Fig. 4).

Since no closed-form solution is available for this problem, we have done several numerical attempts to correctly solve it. These attempts are based on the definition of special singular elements that exploit some of the properties of classical singular elements defined in [5] (see Table I, Section III and IV). In particular, with reference to Fig. 15, we tried several schemes based on lacunary singular elements:

i) *half-edge* (***he***) singular element in sheet 2 connected to regular elements in sheets 1 and 3;
ii) edge-singular element in sheet 2 connected to edge-aligned *weak half-vertex* (***whv***) singular elements in sheets 1 and 3;
iii) edge-singular element in sheet 2 connected to edge-aligned *strong half-vertex* (***shv***) singular elements in sheets 1 and 3;
iv) same as iii) but with non-edge-aligned *strong half-vertex* (***shv***) singular elements in sheets 1 and 3.

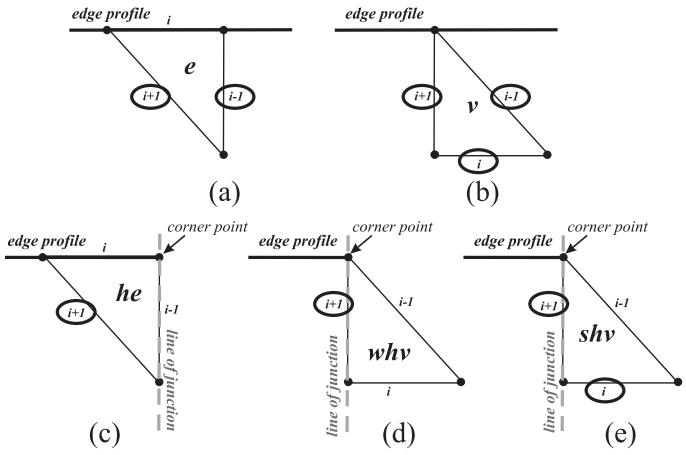

Fig. 16. Classical and lacunary singular elements to model plate-to-surface junctions. The circles highlight the edge dummy indexes on which are based the singular functions that need to be included to define: an edge (***e***) singular element (Fig. 16a), a vertex (***v***) singular element (Fig. 16b), a *half-edge* (***he***) singular element (Fig. 16c), a *weak half-vertex* (***whv***) singular element (Fig. 16d), a *strong half-vertex* (***shv***) singular element (Fig. 16e).

The lacunary singular elements are formed by the union of a vector subset of regular basis functions of order p plus: an incomplete vector subset of edge singular basis functions of order s for (***he***) element; an incomplete vector subset of vertex singular basis functions of order s for (***whv***) and (***shv***) elements. In Fig. 16 we highlight with circles the edge dummy indexes on which are based the singular functions that need to be included to define: an edge (***e***) singular element (Fig. 16a), a vertex (***v***) singular element (Fig. 16b), a *half-edge* (***he***) singular element (Fig. 16c), a *weak half-vertex* (***whv***) singular element (Fig. 16d), a *strong half-vertex* (***shv***) singular element (Fig. 16e).

All the proposed schemes yield a smooth transition for the current around the line of junction, but only scheme iii) yields full convergence.

With reference to Fig. 4, in scheme i) T3 is an *half-edge* singular element, *i.e.* lacunary edge-singular element, where the singular bases interpolating the line of junction are removed. Cells T1 to T6 (except T3) are regular elements.

With reference to Fig. 4, in scheme ii), iii) and iv) T3 is a singular-edge element, while cells T1 and T2 are *half-vertex* singular elements, *i.e.* lacunary vertex-singular elements, where vertex singular basis functions interpolating the line of junction are added to the regular basis subset. Cells T4, T5, T6 are regular elements.

Schemes iii) and iv) differ from scheme ii) because they include the edgeless (element-based) vertex singular basis functions ${}^{v}\mathbf{V}_i$ [5] in the singular subsets of the *half-vertex* singular elements. For this reason, elements of scheme iii) and iv) are labeled *strong half-vertex* singular elements, while elements of scheme ii) are labeled *weak half-vertex* singular elements. Scheme iii) and iv) differ in the topological

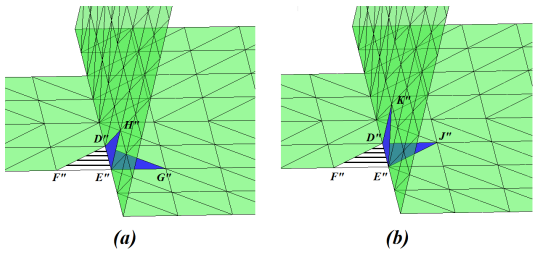

Fig. 17. Junction connection of three elements involving the sharp edge: the triangular elements with sharp edge is in stripe pattern, the two connected triangles are in blue. (a) and (b) shows two connected elements that are respectively not *edge-aligned* and *edge-aligned*. (a) and (b) are respectively partial view of mesh **D** and mesh **MD**.

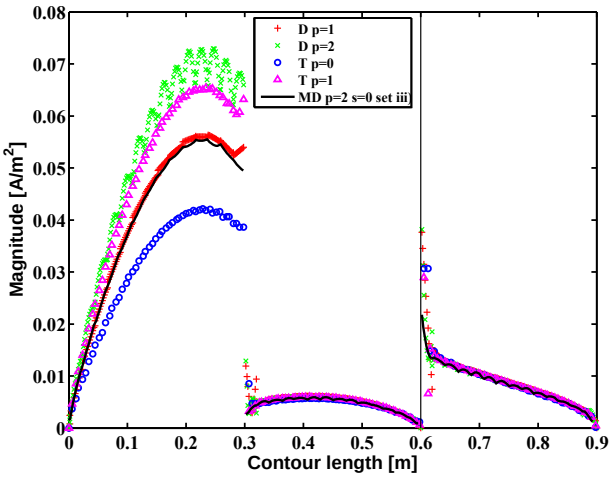

Fig. 18. Modified T-shape structure illuminated at 300MHz by a plane wave with $\theta^i = 45^o$, $\varphi^i = -75^o$ and $\mathbf{E_0} = 1\hat{\theta}$ [V/m]. Magnitude of current density component tangent to the contour line A" $\rightarrow$ B" and E" $\rightarrow$ C" and sampled at a distance of $\lambda/1000$ in z direction from the border of the structure, see also Fig. 15. Simulations obtained with regular elements and different meshes are compared with the reference simulation obtained with mesh **MD** and singular set iii) of order $p = 2, s = 0$.

properties of the geometrical discretization inside the surface. With reference to Fig. 4, the lacunary *half-vertex* singular elements T1 and T2 are said to be *edge-aligned* if the edge of T1 and T2 opposite to the corner node is perpendicular to the height vector of the knife edge of T3, see Fig. 17. This geometrical property influences the modeling properties of the vertex singular basis subset, since the singularity is modeled through the properties of the parent coordinates [5].

Fig. 17a shows mesh **D** in the transition region where a triangular element with the sharp edge is in stripe pattern and the two connected triangles are colored in blue. In this case the transition regions may be modeled with the singular bases defined in i) and iv). Fig. 17b shows mesh **MD** which is a locally modified version of mesh **D** in the transition region where the connected triangles inside the smooth surface are *edge-aligned*, thus the transition regions may be modeled with the singular bases defined in ii) and iii).

In scheme i) or, in general, for triangular elements not lying on the sharp edge profile, the modeling procedure of the junction is limited to regular DOFs. For subsets ii), iii), iv) we have to enforce KCL and conformity to singular basis functions in lacunary singular elements, as stated in Section II. Conformity among singular basis functions is fully studied in [5], while KCL involves relations among singular DOFs defined at interpolation nodes of the line of junction, thus no constraint is imposed on the edgeless basis functions ${}^v\mathbf{V}_i$ if included.

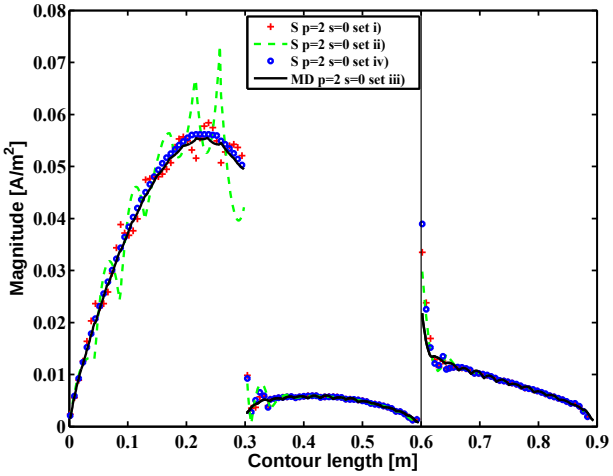

Fig. 19. Magnitude of current density component tangent to the contour lines A" $\rightarrow$ B" and E" $\rightarrow$ C" and sampled at a distance of $\lambda/1000$ in z direction from the border of the structure when the structure is illuminated by a plane wave with $\theta^i = 45^o$, $\varphi^i = -75^o$ and $\mathbf{E_0} = 1\hat{\theta}$ [V/m] at 300MHz. The figure show comparison among numerical results obtained by the four schemes proposed in Section IV. The reference simulation is the one obtained with mesh **MD** and singular set iii) of order $p = 2, s = 0$.

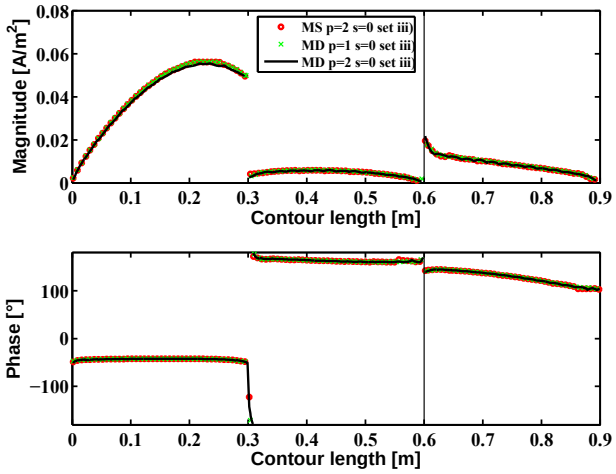

Fig. 20. Study of convergence of the reference (best) singular scheme iii) in terms of magnitude and phase of the current density tangent to the contour lines A" $\rightarrow$ B" and E" $\rightarrow$ C" and sampled at a distance of $\lambda/1000$ in z direction from the border of the structure, see also Fig. 15.

To illustrate the effectiveness of the proposed procedure we present several results obtained in the frequency domain applying the Galerkin method to the EFIE. We have deeply investigated the modified T-shape structure (Fig. 15) in free space illuminated by a linearly polarized plane wave (4) with

parameters $\theta^i = 45^o$, $\varphi^i = -75^o$ and $\mathbf{E_0} = 1\hat{\theta}$ [V/m] at 300MHz (*i.e.* sheet 1 and 3 is $0.3\lambda \times 0.1\lambda$ while sheet 2 is $0.3\lambda \times 0.05\lambda$). Numerical results are obtained with regular elements and modified singular elements with five different meshes: mesh **S**,**MS**,**D**,**MD**,**T** respectively with 140, 140, 560, 560, and 1260 right-angled triangular elements of the same size. Mesh **MS** is a locally modified version of mesh **S** in the transition region to get edge-aligned lacunary vertex elements inside the smooth surface, as done for mesh **MD**. In the following, we consider as reference (best) solution the one obtained for mesh **MD** and scheme iii) of order $(p = 2, s = 0)$.

Figs. 18, 19 and 20 show the current density component tangent to the contour line A" $\rightarrow$ B" and E" $\rightarrow$ C" and sampled at a distance of $\lambda/1000$ in z direction from the border of the structure (see Fig. 15 for the contour line). This component is strongly affected by the bifurcation of the structure since it is normal to the line of junction. Fig. 18 shows that the solutions obtained by using regular basis functions with the enforcement of junction condition are not able to model the problem. The figure shows unstable solutions with unphysical oscillations of the current density at wrong scale of magnitude near the sharp edge profile and the junction. Fig. 19 shows that, the use of schemes i) and ii) yields still incorrect solutions with unphysical oscillations in the entire sharp edge region and junction. This means that the solution is unstable. Fig. 20 demonstrates that scheme iii) converges to a stable and physical solution. Moreover Fig. 19 shows also that the use of scheme iv), which is different from iii) only for geometrical properties, yields a convergent sub-optimal solution that is locally unsatisfactory along the line of junction. Table II reports details on the number of DOFs for all the performed simulations in this Section (in agreement with the discussion reported in Section II).

Definitely, in order to model properly sharp edge plates joined to a smooth surface we need lacunary vertex singular elements inside the smooth surface that are capable of modeling normal-to-edge and tangent-to-edge components of the current density, *i.e. strong half-vertex* singular elements.

TABLE II
NUMBER OF DOFS IN SIMULATIONS OF SECTION IV

Bases and Mesh	DOFs	Figure
p=1, mesh **D**	2700	Fig. 18
p=2, mesh **D**	5730	Fig. 18
p=0, mesh **T**	1815	Fig. 18
p=1, mesh**T**	6150	Fig. 18
set i) p=2,s=0, mesh **S**	1520	Fig. 19
set ii) p=2,s=0, mesh **S**	1524	Fig. 19
set iv) p=2,s=0, mesh **S**	1528	Fig. 19
set iii) p=2,s=0, mesh **MS**	1528	Fig. 20
set iii) p=1,s=0, mesh **MD**	2995	Fig. 20
set iii) p=2,s=0, mesh **MD**	6025	Figs. 18,19,20

V. CONCLUSIONS

A complete procedure to handle junctions in complex structures constituted by thin metallic plates such as wings, fins, winglets is proposed in the framework of surface integral equation methods. The approach is based on the use of divergence-conforming higher-order interpolatory vector basis functions, singular vector basis functions and on Kirchhoff's Current Law. The additive nature of the bases permits the definition of lacunary singular elements that model structures containing sharp edge plates and smooth surfaces. In this paper we have described the modeling procedure with the definition of the required basis functions and unknowns. The paper presents several numerical test cases based on the canonical T-shape surface junction and its variants that show the instability of solutions obtained using classical methods and the full convergence of the proposed numerical procedure.

REFERENCES

[1] R.D. Graglia, D.R. Wilton, and A.F. Peterson, "Higher order interpolatory vector bases for computational electromagnetics," *IEEE Trans. Antennas Propagat.,* vol. 45, no. 3, pp. 329–342, Mar. 1997.

[2] R.D. Graglia, G. Lombardi, "Singular higher order complete vector bases for finite methods," *IEEE Trans. Antennas Propagat.,* vol.52, no.7, pp. 1672-1685, Jul. 2004.

[3] R.D. Graglia, and G. Lombardi, "Vector functions for singular fields on curved triangular elements, truly defined in the parent space," in *Proc. IEEE AP-S Int. Symp.,* vol. 1, San Antonio, TX, June 2002, pp. 6265.

[4] R.D. Graglia, G. Lombardi, D.R. Wilton, W.A. Johnson, "Modeling edge singularities in the method of moments," in *Proc. IEEE AP-S Int. Symp.,* vol. 3A, 3-8 Jul 2005, pp. 56-59.

[5] R.D. Graglia, G. Lombardi, "Singular Higher Order Divergence-Conforming Bases of Additive Kind and Moments Method Applications to 3D Sharp-Wedge Structures," *IEEE Trans. Antennas Propagat.,* vol.56, no.12, pp. 3768-3788, Dec 2008

[6] G. Lombardi, and R.D. Graglia, "Singular higher order vector bases for wedge-structure MoM-models: The simple recipe," in *Proc. International Conference on Electromagnetics in Advanced Applications (ICEAA),* Torino, Italy, 14-18 Sept. 2009, pp. 1082-1085.

[7] D. Erricolo, R.D. Graglia, G. Lombardi, T. Stoia, and P.L.E. Uslenghi, "Benchmark targets for Computational Electromagnetics programs modeling structures with edges," in *Proc. IEEE AP-S Int. Symp.,* 11-17 Jul 2010, pp.1-4.

[8] B. M. Kolundzija, "Electromagnetic modeling of composite metallic and dielectric structures," *IEEE Trans. Microw. Theory Techn.,* vol.47, no.7, pp.1021-1032, Jul 1999

[9] J. Shin, A. W. Glisson, and A. A. Kishk, "Modeling of general surface junctions of composite objects in an SIE/MoM formulation," in *Proc. ACES Conf.,* 2000, pp. 683–690.

[10] M. A. Carr, E. Topsakal, J. L.Volakis, and D. C. Ross, "Adaptive integral method applied to multilayer penetrable scatterers with junctions," in *Proc. IEEE AP-S Int. Symp.,* 2001, vol. 4, pp. 858–861.

[11] M. Carr, E. Topsakal, J.L. Volakis, "A procedure for modeling material junctions in 3-D surface integral equation approaches," *IEEE Trans. Antennas Propagat.,* vol.52, no.5, pp. 1374–1378, May 2004.

[12] P. Yla-Oijala, M. Taskinen, and J. Sarvas, "Surface integral equation method for general composite metallic and dielectric structures with junctions," *Progress In Electromagnetics Research,* Vol. 52, 81–108, 2005.

[13] F. Vipiana, D.R. Wilton, "Optimized Numerical Evaluation of Singular and Near-Singular Potential Integrals Involving Junction Basis Functions," *IEEE Trans. Antennas Propagat.,* vol.59, no.1, pp.162–171, Jan. 2011.

[14] S.M. Rao, D.R. Wilton, A.W. Glisson, "Electromagnetic scattering by surfaces of arbitrary shape," *IEEE Trans. Antennas Propagat.,* vol. 30, pp.409-418, May 1982.

[15] J. Meixner, "The behavior of electromagnetic fields at edges," *IEEE Trans. Antennas Propagat.,* vol. 20, no. 4, pp. 442-446, Jul 1972.

[16] J. Van Bladel, *Singular Electromagnetic Fields and Sources.* Oxford, U. K.: Clarendon, 1991.

[17] R.D. Graglia, G. Lombardi, "Machine Precision Evaluation of Singular and Nearly Singular Potential Integrals by Use of Gauss Quadrature Formulas for Rational Functions," *IEEE Trans. Antennas Propagat.,* vol.56, no.4, pp.981-998, Apr 2008

[18] G. Lombardi, "Design of quadrature rules for Müntz and Müntz-logarithmic polynomials using monomial transformation," *International Journal for Numerical Methods in Engineering,* pp. 1687-1717, Vol. 80, n.13, 2009

Guido Lombardi (S'02-M'03-SM'11-) was born in Florence, Italy, on December 8, 1974. He received the Laurea degree (*summa cum laude*) in telecommunications engineering from the University of Florence, Italy, in 1999 and the Ph.D. degree in electronics engineering at the Polytechnic of Turin, Italy, in jan. 2004. In 2000-01, he was officer of the Italian Air Force. In 2004 he was an Associate Researcher with the Department of Electronics of Polytechnic of Turin and in 2005 he joined the same Department as an Assistant Professor with tenure. He was the recipient of the Raj Mittra Travel Grant award for junior researcher at 2003 IEEE AP-S International Symposium and USNC/CNC/URSI National Radio Science Meeting, Columbus, OH, USA. In the same year he was Visiting Researcher at the Department of Electrical and Computer Engineering, University of Houston, Houston, TX, USA.

His research interests comprise analytical and numerical methods for electromagnetics, Wiener-Hopf method, diffraction, theoretical and computational aspects of FEM and MoM, numerical integration, electromagnetic singularities, waveguide problems, microwave passive components, project of orthomode transducers (OMT), metamaterials.

He is an associate editor of the IEEE ACCESS journal. He served as member of the Organizing Committee and the Technical Program Committee in the International Conference on Electromagnetics in Advanced Applications (ICEAA) since the 2001 edition and in the IEEE-APS Topical Conference on Antennas and Propagation in Wireless Communications (IEEE-APWC) since the 2011 edition. He was Publication Chair of ICEAA and IEEE-APWC in 2011, 2013-2014 editions. He served the 2012 IEEE AP-S International Symposium and USNC/CNC/URSI National Radio Science Meeting, Chicago, IL, USA as co-organizer of the Special Session entitled "Challenging Canonical Scattering Problems and New EM Problems involving Special Materials".

He regularly serves as a reviewer of several international journals on physics, electrical engineering and electromagnetics, among which IEEE, IET, Wiley, Elsevier Journals and Transactions.

Roberto D. Graglia (S'83-M'83-SM'90-F'98) was born in Turin, Italy, on July 6, 1955. He received the Laurea degree (*summa cum laude*) in electronic engineering from the Polytechnic of Turin in 1979, and the Ph.D. degree in electrical engineering and computer science from the University of Illinois at Chicago in 1983. From 1980 to 1981, he was a Research Engineer at CSELT, Italy, where he conducted research on microstrip circuits. From 1981 to 1983, he was a Teaching and Research Assistant at the University of Illinois at Chicago. From 1985 to 1992, he was a Researcher with the Italian National Research Council (CNR), where he supervised international research projects. In 1991 and 1993, he was Associate Visiting Professor at the University of Illinois at Chicago. In 1992, he joined the Department of Electronics and Telecommunications, Polytechnic of Turin, as an Associate Professor. He has been a Professor of Electrical Engineering at that Department since 1999. He has authored over 150 publications in international scientific journals and symposia proceedings. His areas of interest comprise numerical methods for high- and low-frequency electromagnetics, theoretical and computational aspects of scattering and interactions with complex media, waveguides, antennas, electromagnetic compatibility, and low-frequency phenomena. He has organized and offered several short courses in these areas.

Since 1997, he has been a Member of the editorial board of ELECTROMAGNETICS. He is a past associate editor of the IEEE TRANSACTIONS ON ANTENNAS AND PROPAGATION, of the IEEE TRANSACTIONS ON ELECTROMAGNETIC COMPATIBILITY, and of the IEEE ANTENNAS AND WIRELESS PROPAGATION LETTERS. He was the Guest Editor of a special issue on Advanced Numerical Techniques in Electromagnetics for the IEEE TRANSACTIONS ON ANTENNAS AND PROPAGATION in March 1997. He has been Invited Convener at URSI General Assemblies for special sessions on Field and Waves in 1996, Electromagnetic Metrology in 1999, and Computational Electromagnetics in 1999. He served the International Union of Radio Science (URSI) for the triennial International Symposia on Electromagnetic Theory as Organizer of the Special Session on Electromagnetic Compatibility in 1998 and was the co-organizer of the special session on Numerical Methods in 2004. Since 1999, he has been the General Chairperson of the International Conference on Electromagnetics in Advanced Applications (ICEAA), and, since 2011, he has been the General Chairperson of the IEEE-APS Topical Conference on Antennas and Propagation in Wireless Communications (IEEE-APWC).

Dr. Graglia is the 2014 President-Elect of the IEEE Antennas and Propagation Society; he has been a member of IEEE AP-S AdCom for the triennium 2006-2008 and an IEEE AP-S Distinguished Lecturer (2009-2012).